Construction of multilayers of bare and Pd modified gold nanoclusters and their electrocatalytic properties for oxygen reduction

2011 Sci. Technol. Adv. Mater. 12 044606

(http://iopscience.iop.org/1468-6996/12/4/044606)

IOP Publishing Science and Technology of Advanced Materials
Sci. Technol. Adv. Mater. **12** (2011) 044606 (10pp) doi:10.1088/1468-6996/12/4/044606

Construction of multilayers of bare and Pd modified gold nanoclusters and their electrocatalytic properties for oxygen reduction

Motoko Harada[1], Hidenori Noguchi[1,2,3], Nikolas Zanetakis[1], Satoru Takakusagi[1,4], Wenbo Song[1,5] and Kohei Uosaki[1,2,3]

[1] Division of Chemistry, Graduate School of Science, Hokkaido University, Sapporo 060-0810, Japan
[2] International Center for Materials Nanoarchitectonics (MANA), National Institute for Materials Science (NIMS), Tsukuba 305-0044, Japan
[3] Global Research Center for Environment and Energy based on Nanomaterials Science (GREEN), National Institute for Materials Science (NIMS), Tsukuba 305-0044, Japan

E-mail: UOSAKI.Kohei@nims.go.jp

Received 28 February 2011
Accepted for publication 17 April 2011
Published 7 July 2011
Online at stacks.iop.org/STAM/12/044606

Abstract
Multilayers of gold nanoclusters (GNCs) coated with a thin Pd layer were constructed using GNCs modified with self-assembled monolayers (SAMs) of mercaptoundecanoic acid and a polyallylamine hydrochloride (PAH) multilayer assembly, which has been reported to act as a three-dimensional electrode. SAMs were removed from GNCs by electrochemical anodic decomposition and then a small amount of Pd was electrochemically deposited on the GNCs. The kinetics of the oxygen reduction reaction (ORR) on the Pd modified GNC/PAH multilayer assembly was studied using a rotating disk electrode, and a significant increase in the ORR rate was observed after Pd deposition. Electrocatalytic activities in alkaline and acidic solutions were compared both for the GNC multilayer electrode and Pd modified GNC electrode.

Keywords: gold nanocluster, self-assembled monolayer (SAM), oxygen reduction reaction (ORR)

1. Introduction

Improvement of the rate of electrochemical reduction of oxygen is essential for the realization of highly efficient fuel cells, because the overpotential for oxygen reduction is relatively large compared with that for hydrogen oxidation, even for noble metals such as Pt. The associated reactions are rather complex [1, 2], and have been studied on examples of well-defined surfaces, including single crystals of Au [3], Ru [4] and Pt [5, 6].

Many researchers have been developing efficient electrocatalysts for the oxygen reduction reaction (ORR) and one of the most promising approaches is to design a bimetallic electrocatalyst [7–17]. Watanabe and Motoo proposed the concept of adatom [7, 8]. Electrochemical deposition of various noble metals such as Ru, Rh and Pd on Pt was carried out to obtain a highly active electrode [9–15].

Pd is one of the most important metals for many electrocatalytic applications. Electrochemical properties of Pd submonolayer on a foreign metal electrode are quite different from those of the bulk Pd electrode. Formation and reduction of Pd oxide from the Pd submonolayer on Au(111) and Au(100) surfaces take place at more and less positive potentials, respectively, than those of the bulk Pd

[4] Present address: Catalysis Ressearch Center, Hokkaido University, Sapporo 001-0021, Japan.
[5] Present address: College of Chemistry, Jilin University, Changchun 130012, China.

and Pd multilayers on Au(111) and Au(100) surfaces and the electrocatalytic activity of formaldehyde oxidation is highest when the Pd coverage is less than a monolayer [16]. The electrocatalytic oxygen reduction has also been investigated at Au(111) [12] and Pt(111) [13, 14] electrodes modified with thin Pd layers. Electrocatalytic activity for the ORR strongly depends on the Pd layer thickness, and higher reduction rates were observed for the electrodes with lower amounts of deposited Pd. To clarify the origin of the unique electrocatalytic properties of a thin Pd layer on a gold single crystal surface, the interfacial geometric and electronic structures of the Pd thin film/Au single crystal electrode were studied by surface x-ray scattering (SXS) [17,18] and second harmonic generation (SHG) spectroscopy [19], respectively. Although Pd forms pseudomorphic layers on Au(111) for a few layers [17] and on Au(100) for over 20 layers [18], the unique electrochemical characteristics were observed only for the gold electrodes covered with a submonolayer of Pd. This observation suggests the importance of electronic effect that was further confirmed by SHG measurements [19]. Thus, the construction of an electrode of high surface area based on the concept of submonolayer modification by Pd is an interesting approach to develop a highly active electrocatalyst for the ORR.

We have already reported the construction of a multilayer of self-assembled monolayer (SAM) protected gold nanoclusters (GNCs) and polyelectrolyte using electrostatic interaction on gold and indium tin oxide (ITO) surfaces, which acted as three-dimensional electrodes [20–25]. In this study, a three-dimensional electrocatalytic electrode was constructed by careful removal of the SAM by anodic oxidation, followed by the deposition of a small amount of Pd on the surface of GNCs in the multilayer assembly. The kinetics of ORR at this electrode was studied using a rotating disk electrode (RDE). The ORR rate at the GNC multilayer electrode was increased significantly by the Pd modification. Electrocatalytic activities of the GNC and Pd modified GNC multilayer electrodes in alkaline and acidic solutions were examined.

2. Experimental

2.1. Materials

Hydrogen tetrachloaurate ($HAuCl_4$, 99.99%), sodium tetrahydroborate ($NaBH_4$), ethanol (superpure grade), toluene (spectroscopy grade), hexanethiol (C_6SH, superpure grade) and sulfuric acid (ultrapure grade) were purchased from Wako Pure Chemicals. Tetra-n-octyl ammonium bromide was obtained from Tokyo Kasei Kogyo, and 11-mercaptoundecanoic acid (MUA, 97%) and polyallylamine hydrochloride (PAH) were supplied by Aldrich. Ferrocenyl alkanethiol (FcC_8SH) was synthesized by a previously reported method [26]. Ultrapure water was produced with a Milli-Q water purification system (Millipore), and ultrapure Ar (99.999%) and O_2 (99.5%) gases were purchased from Air Water.

2.2. Synthesis of SAM protected GNCs

GNCs covered by C_6SH, FcC_8SH and MUA SAMs (MHF-GNCs) were prepared by the procedure reported previously [20–25]: C_6SH SAM protected GNCs were synthesized by the two-phase method of Brust *et al* [27]. Then, FcC_8SH and MUA were introduced sequentially onto the surface of the C_6SH SAM protected GNCs by the place exchange method [28]. Here, FcC_8SH was used as a probe to estimate the amount of GNC in the multilayer during the oxidative removal of SAM by measuring the redox charge of the ferrocene group, and MUA acted as a binder based on the carboxylate/PAH/carboxylate electrostatic interaction. The molar ratio of C_6SH : FcC_8SH : MUA on the MHF-GNCs surface was estimated by ^{1}H-NMR (Hitachi, R-1900, 90 MHz) as 28 : 12 : 60. The core size of the MHF-GNCs was estimated as 1.8 nm by transmission electron microscopy (TEM)(JEOL, JEM-200FX) [22, 23].

2.3. Electrochemical measurements

We employed a three-electrode electrochemical cell with a hanging meniscus configuration. A Pt wire and Ag/AgCl (NaCl saturated) were used as counter and reference electrode, respectively. The electrode potential was controlled by a potentiostat/function generator system (Hokuto Denko, HSV-100).

RDE measurements of the ORR were carried out using a dual potentiostat (Hokuto Denko, HR-101B) and a function generator (Hokuto Denko, HB-105). The rotation rate was varied stepwise from 500 to 4500 rpm using a speed control unit (Hokuto Denko, HR-202). ORR was carried out in 0.1 M KOH (pH = 13) and 0.1 M H_2SO_4 (pH = 1) solutions. These solutions were saturated with oxygen by passing oxygen gas through them for at least 1 h. Polarization curves were recorded between −600 and 200 mV in a 0.1 M KOH solution and between −200 and 800 mV in a 0.1 M H_2SO_4 solution, at a scan rate of 10 mV s^{-1}.

All measurements were carried out at room temperature (25 °C) after the electrolyte solution was deaerated by passing Ar gas through it for at least 30 min except for the ORR study. The surface areas of Au(111) electrode and Au RDE were 0.045 and 0.265 cm^2, respectively [29, 30].

2.4. Preparation of the multilayer of SAM protected GNCs

A gold single crystal bead was prepared from a gold wire (99.999%, diameter 1 mm, Tanaka Precious Metals) by Clavilier's method [31]. It was cut parallel to the (111) facet, mechanically polished using 0.5 μm diamond slurry (Maruto) and annealed at 800 °C for 8 h in an electric furnace (Denken, KDF-S-70) under ultrapure N_2 atmosphere. Before the preparation of SAM protected GNCs, the electrode surfaces were treated as follows. The gold single crystal was annealed in a hydrogen flame and gradually cooled in a nitrogen stream. An ITO substrate was cleaned by immersing it in a 3 : 1 H_2SO_4 (conc.)-H_2O_2 (30%) solution for 5 s, then thoroughly rinsed with Milli-Q water and finally dried in ultrapure nitrogen. A gold RDE was polished to a mirror finish

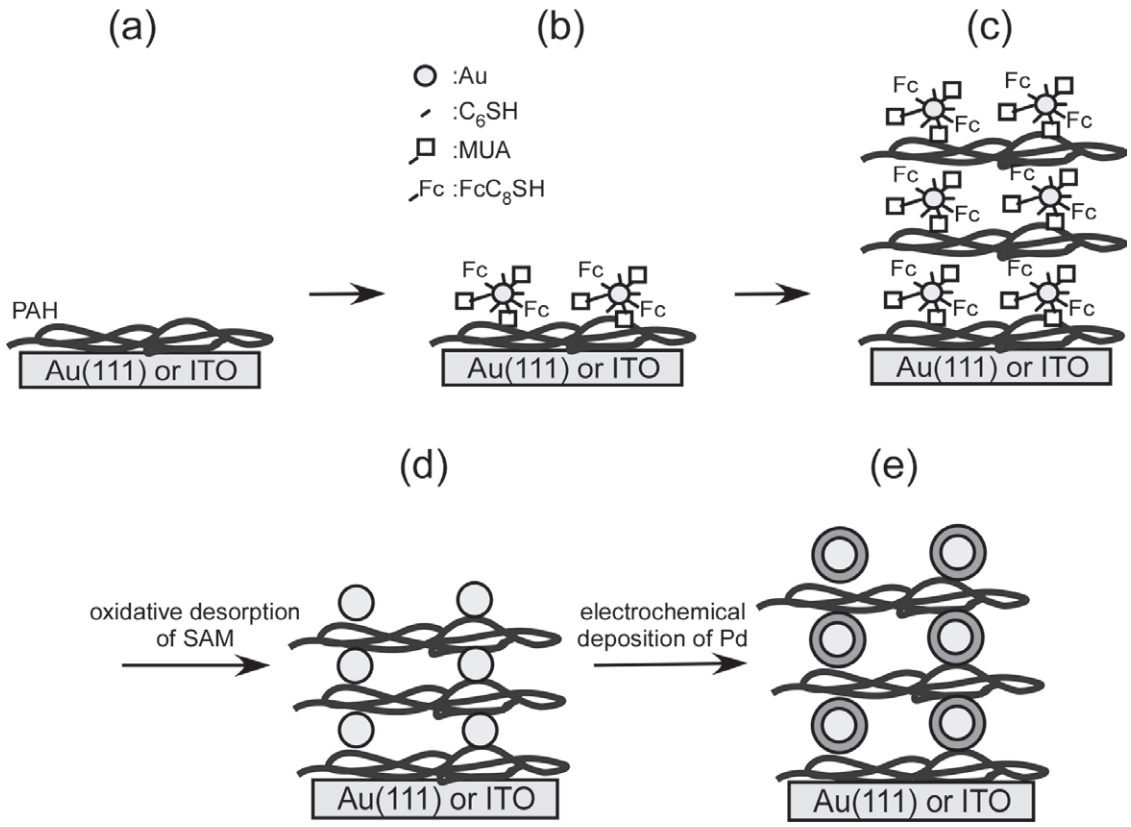

Scheme 1. Preparation of a multilayer of SAM modified bare and Pd modified GNCs on Au and ITO electrodes. (a) PAH modification, (b) formation of the monolayer of SAM modified GNCs, (c) formation of the multilayer of SAM modified GNCs, (d) removal of the SAMs from the GNCs and (e) adsorption of Pd on the GNCs.

with 3.0 μm diamond slurry (Maruto) and cleaned by rinsing with Milli-Q water. Then, oxidation reduction cycles between −200 and 1450 mV were applied in a 0.1 M H_2SO_4 solution at a scan rate of 200 mV s^{-1} for about 2 h. Multilayers of SAM protected GNCs were prepared on gold and ITO surfaces. The substrate was dipped first in a 0.1 M NaOH aqueous solution containing 2 mg mL^{-1} PAH for 5 min and then in an ethanol solution containing 0.15 wt% GNCs for 15 min, with a rinse after each dip. The PAH/GNC dipping cycle was repeated to obtain the PAH/GNC multilayer as shown in scheme 1(a)–(c) [21–25].

2.5. Removal of SAMs from and deposition of Pd on the GNC surfaces in the multilayer

SAMs were removed from GNC surfaces by electrochemical oxidative desorption repeating the potential cycles between 0 and 1300 mV in a 0.1 M $HClO_4$ solution with a scan rate of 50 mV s^{-1} (Scheme 1(d)) [24]. After each potential cycle, a CV was recorded between 0 and 800 mV to monitor the redox response of the ferrocene group and evaluate the amount of remaining SAMs on the GNC surface. The oxidative desorption of SAMs from the GNC surface was also monitored by observing the surface of the ITO electrode (1 × 0.5 cm) covered with the multilayer of the SAM protected GNCs/PAH in a field emission scanning electron microscope (FE-SEM, Hitachi, 5200-S) at an acceleration voltage of 25 keV.

After confirming the complete removal of SAMs, Pd was electrodeposited on the surface of the GNCs in the multilayer by stepping the potential from 850 to 200 mV in a 0.1 M H_2SO_4 solution containing 0.1 mM $PdCl_4$ (Scheme 1(e)) [24]. The deposition time was adjusted to pass the charge corresponding to the monolayer coverage of GNCs. Electrochemical measurements in Ar saturated solutions were also carried out after the oxidative desorption of SAMs and further Pd deposition.

3. Results and discussion

3.1. Oxidative desorption of SAMs from the multilayer of PAH/SAM protected GNCs

The solid line in figure 1(a) shows a CV of a 5-layer GNC electrode on a Au(111) electrode in a 0.1 M $HClO_4$ solution (scan rate 50 mV s^{-1}). The oxidation/reduction wave of the ferrocence group attached to the GNCs was observed at around 380 mV. The redox process of the surface attached ferrocene group can be expressed as [26, 32, 33],

$$-\mathrm{Fc} + \mathrm{X}^- \rightarrow -\mathrm{Fc}^+\mathrm{X}^- + \mathrm{e}^-, \qquad (1)$$

where −Fc and $-Fc^+$ represent the neutral and oxidized states of the ferrocene group, respectively, $^-X^-$ is an anion in solution, and $-Fc^+X^-$ is an ion pair between the ferricenium cation and the anion.

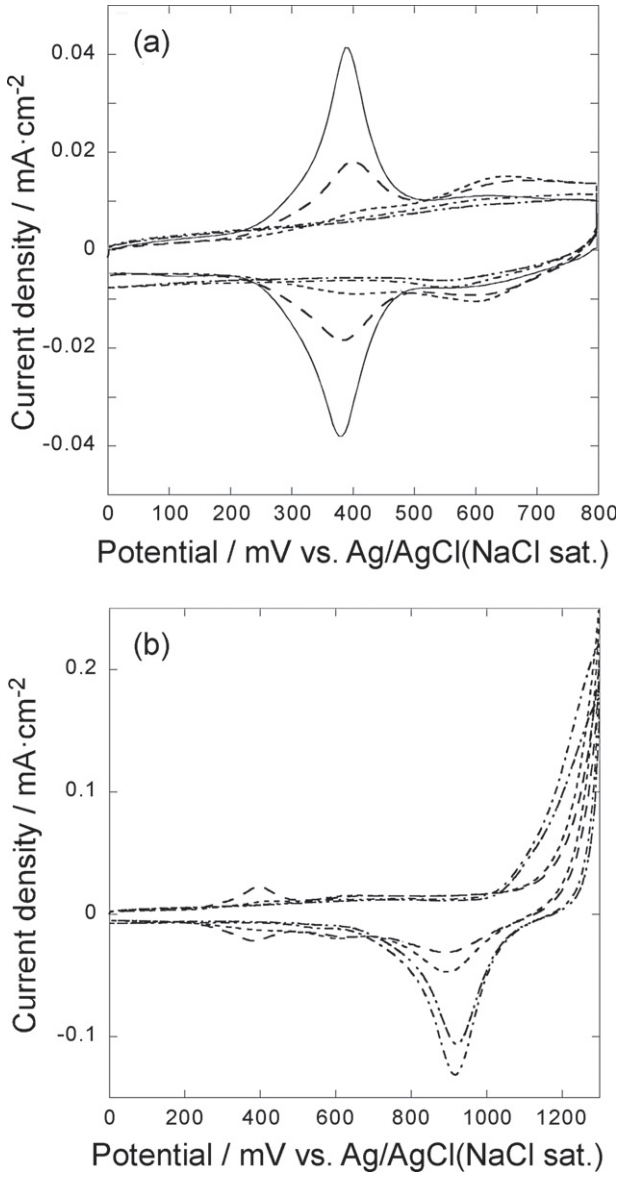

Figure 1. (a) Cyclic voltammograms of the 5-layer GNC electrode on the Au(111) electrode measured in an Ar saturated 0.1 M $HClO_4$ solution at a scan rate of 50 mV s^{-1}: (—) 0, (– –) 5, (····) 10, (–··–) 20, (–·–) 30 cycles between 0 and 1300 mV were applied to desorb SAM. (b) Cyclic voltammograms of oxidative desorption of SAM from 5 layers of the GNC electrode on the Au(111) electrode measured in an Ar saturated 0.1 M $HClO_4$ solution at a sweep rate of 50 mV s^{-1}, repeating the potential cycle between 0 and 1300 mV for 5 (– –), 10 (····), 20 (–··–), and 30 (–·–) times to desorb SAM.

Figure 1(b) shows CVs of the 5-layer GNC electrode on the Au(111) electrode in a 0.1 M $HClO_4$ solution when the potential was scanned between 0 and 1300 mV at a rate of 50 mV s^{-1}. In the positive going scan a large anodic current was started to be observed at around 1000 mV and a small cathodic peak was observed at around 950 mV in the negative going scan. The cathodic peak should be due to the reduction of gold oxide. As the potential cycle was repeated, the anodic current started to flow from more negative potential, and the charge of the cathodic peak increased up to 25 cycles and then decreased. The wave due to the redox of the ferrocene moiety decreased as the potential cycle was repeated and disappeared after about 20 cycles. These results show that the anodic current was due to both the formation of Au oxide and anodic oxidation of the SAMs at the GNC surface, which proceeds as follows [34]:

$$R\text{–}(CH_2)_2S\text{–}Au + 3H_2O \rightarrow R\text{–}(CH_2)_2SO_2OH + 5H^+ + Au + 5e^-, \quad (2)$$

$$R\text{–}(CH_2)_2SO_2OH + 3H_2O \rightarrow R\text{–}(CH_2)\text{–}COOH + HSO_4^- + 7H^+ + 6e^-, \quad (3)$$

$$R\text{–}(CH_2)\text{–}COOH + 2H_2O \rightarrow R\text{–}COOH + CO_2 + 6H^+ + 6e^-. \quad (4)$$

Initially, the GNC surfaces were covered with SAMs and the oxidative decomposition proceeded at positive potentials. As the potential cycle was repeated, the SAMs were gradually removed, exposing larger areas of the gold surface and thereby increasing the charge for the gold oxide reduction. After 20–25 cycles, the SAMs were totally removed and a small decrease in the charge for the gold oxide reduction was observed, suggesting a small decrease in the surface area, i.e. the aggregation of the GNCs. The decrease in the charge was gradual, revealing that the GNCs did not aggregate significantly even after the SAMs were removed.

FE-SEM was used to examine the size of the GNCs after the oxidative desorption of the SAMs. Figure 2 shows the FE-SEM images of 5 layers of GNCs/PAH on an ITO surface after up to 15 oxidative desorption cycles in a 0.1 M $HClO_4$ solution at a scan rate of 50 mV s^{-1}. The 50–100 nm sized grains observed in all images originate from the ITO surface. The GNC size before the oxidative desorption was estimated as 1.8 nm by TEM, which was too small to be observed by the present FE-SEM measurements [22, 23]. After repeating the potential cycles for oxidative desorption of the SAMs, the GNCs became visible in the FE-SEM images because of the aggregation of GNCs. The average diameters of the GNC clusters reached about 5 nm after 7 cycles (figure 2(d)) and did not change upon further potential cycles.

GNCs in the close vicinity were aggregated because the electrostatic interaction between PAH, i.e. cationic polymer, and GNCs with MUA, i.e. anionic moiety, was lost after oxidative desorption of SAMs. However, the aggregation stopped when the size of GNCs became about 5 nm. This suggests that the energy gain due to the further aggregation was smaller than the energy barrier for the GNCs to be close enough for further growth because GNCs were surrounded by PAH even after MUA was removed.

3.2. Electrochemical deposition of Pd on the surface of bare GNCs within the multilayer

After SAM molecules were oxidatively desorbed from the GNC surfaces, Pd was electrodeposited on the GNCs by stepping the potential from 850 to 200 mV in a 0.1 M H_2SO_4 solution containing 0.1 mM $PdCl_4$. Figure 3 shows the CV

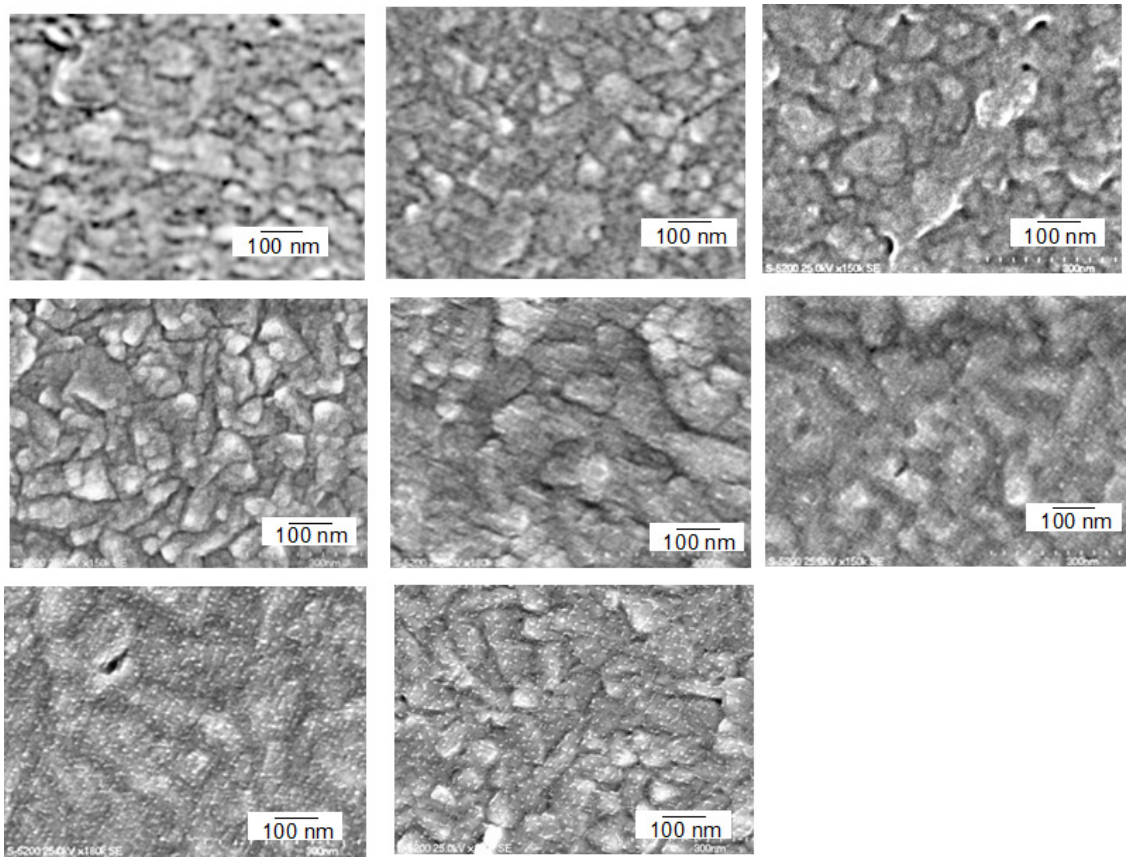

Figure 2. FE-SEM images of (a) ITO, (b) ITO coated with PAH, 5 layers of PAH/GNCs on ITO substrates after (c) 0, (d) 1, (e) 2, (f) 3, (g) 4, and (h) 14 oxidative desorption cycles in a 0.1 M $HClO_4$ solution applied at a scan rate of 50 mV s^{-1}.

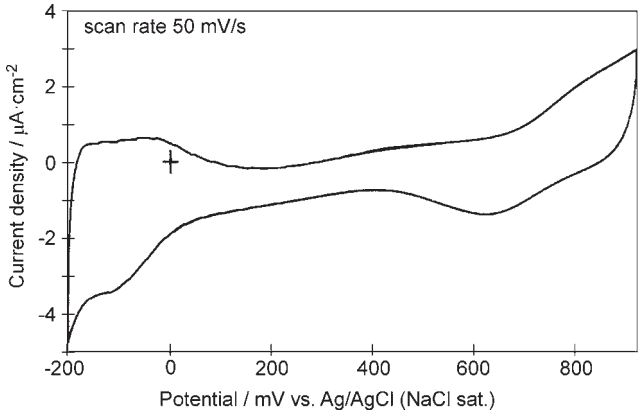

Figure 3. Cyclic voltammogram of the 5-layer Pd modified GNC electrode in a 0.1 M H_2SO_4 solution measured at a scan rate of 50 mV s^{-1}.

of the 5-layer GNC electrode measured in a 0.1 M H_2SO_4 solution after Pd deposition[6]. Hydrogen adsorption and desorption peaks, which were absent before Pd deposition, are observed between −200 and 0 mV, and surface oxide formation and reduction take place at a much more positive potential than before Pd deposition. The amount of Pd deposited on the GNC surface can be estimated from the charge corresponding to the hydrogen adsorption and desorption peaks that was 50 μC cm^{-2}. The charge for the oxide reduction of the 5-layer GNC electrode after 30 oxidative desorption cycles, i.e. bare GNCs, was about 400 μC cm^{-2} (figure 1(b)). Thus, the Pd coverage on the GNCs within the multilayer was estimated to be 25% because hydrogen adsorption/desorption and oxide reduction are 1 and 2 electron processes, respectively. The discrepancy between the values corresponding to Pd deposition (monolayer equivalent) and hydrogen adsorption/desorption may be due to the high double layer charging current at the multilayer modified electrode.

[6] The CV in figure 3 has a background originating from dissolved oxygen within the multilayer. Although the solution was deaerated by passing Ar gas for more than 30 min, dissolved oxygen remained within the multilayer.

3.3. Catalytic activity of the multilayer of bare and Pd modified GNC electrodes in alkaline solution

Figure 4 shows the polarization curves of the 5-layer GNC electrode deposited on a RDE after 35 oxidative desorption cycles. The curves were measured before (figure 4(a)) and after (figure 4(b)) Pd deposition, in an oxygen saturated 0.1 M KOH solution, at a scan rate of 10 mV s^{-1} and a rotation rate between 500 and 4500 rpm as indicated in the figure. Before Pd deposition, cathodic current started to be observed at around −50 mV. It increased as the electrode potential became more negative and then limiting current was observed. The potential where cathodic current started to flow was more

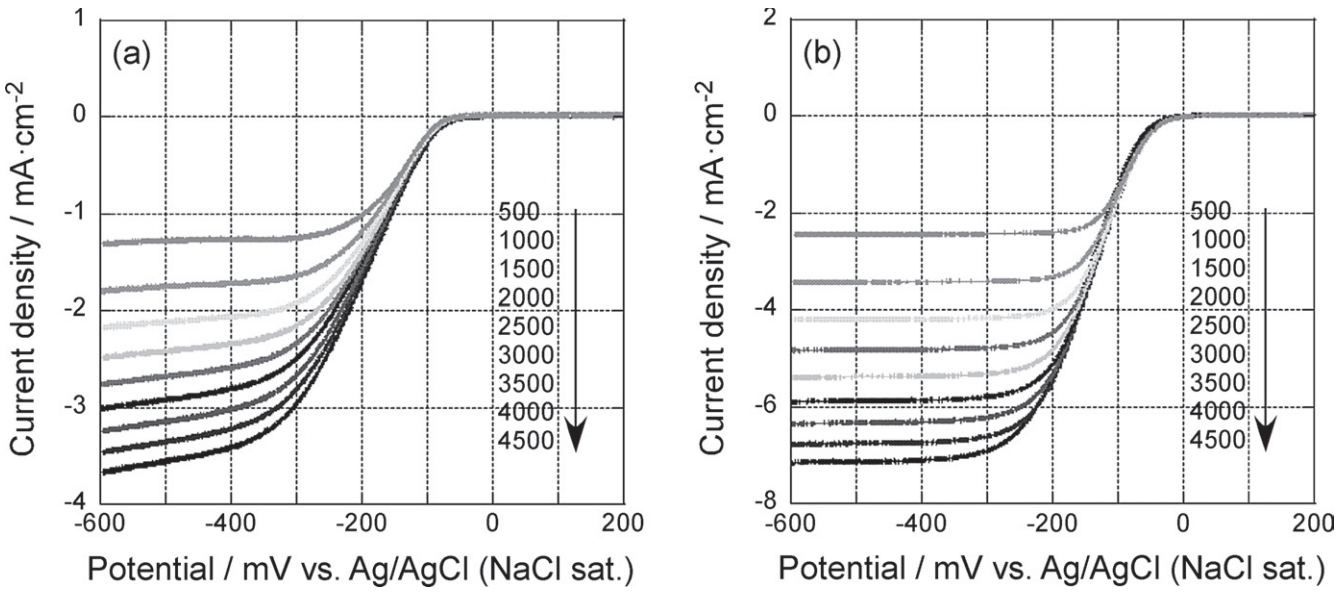

Figure 4. Rotation rate dependent polarization curves of the 5-layer GNC electrode after 35 oxidative desorption cycles (a) before and (b) after Pd deposition. The curves were measured in an oxygen saturated 0.1 M KOH solution at a scan rate of 10 mV s^{-1}.

positive than the values for Au(111) or carbon-supported Au nanoparticles in alkaline solution by about 30 mV [35]. These results show that the ORR activity was higher at the GNC multilayer electrode.

At the Pd modified GNC electrode, cathodic current became observable at around 50 mV. It increased as the potential was scanned to negative direction and reached limiting current at around −300 mV. Although the onset potential was shifted by only about 100 mV after Pd deposition, the limiting current at a given rotation rate of the Pd modified GNC electrode was about twice of that of the bare GNC electrode.

The relationship between the diffusion limited current density and rotation rate is given by the Levich equation as

$$i_L = B\omega^{1/2} = 0.620nFC_{O2}{}^{*}D^{2/3}\omega^{1/2}\upsilon^{-1/6}. \quad (5)$$

Here, i_L is the diffusion limited current, n is the number of electrons transferred in the overall reaction process, F is the Faraday constant (96490 C mol^{-1}), υ is the kinematic viscosity (0.01 cm^2 s^{-1}) [36], D is the diffusion coefficient of oxygen molecules, C_{O2}^{*} is the bulk concentration of oxygen (0.1 M KOH: 1.2×10^{-6} mol cm^{-3}, 0.1 M H_2SO_4: 1.1×10^{-6} mol cm^{-3}) [37, 38] and ω is the rotation rate. The plot of i_L versus $\omega^{1/2}$ is expected to yield a straight line and the number of electrons can be determined from the slope.

Figure 5 shows the Levich plots for the GNC multilayer electrode before and after Pd deposition using the data at −600 mV of figure 4. Linear relations are obtained in both cases with the slopes corresponding to the 2- and 4-electron ORR processes described below for the former and the latter, respectively [39]:

$$O_2 + H_2O + 2e^- \rightarrow HO_2^- + OH^-, \quad (6)$$

$$O_2 + 2H_2O + 4e^- \rightarrow 4OH^-. \quad (7)$$

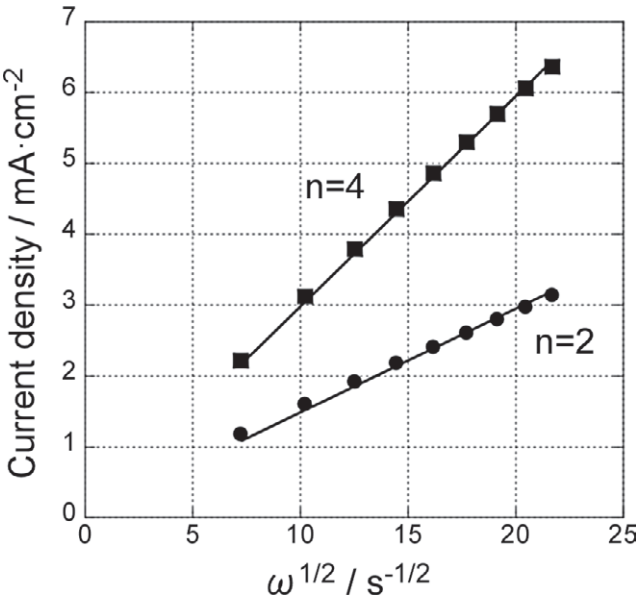

Figure 5. Levich plots for the GNC multilayer electrode at −600 mV before (■) and after (●) Pd deposition (figure 4). Solid lines are fit for 2-electron and 4-electron processes.

Thus, a submonolayer amount of Pd on GNCs significantly enhanced the ORR activity, and the activity of the present Pd modified GNC electrode was superior to those of Pd(111) and carbon-supported Pd nanoparticles [35, 40, 41].

For a more quantitative analysis, one needs to obtain the potential dependent rate constant of the ORR. The current–potential relations can be analyzed with the following Koutecky–Levich (K–L) equation:

$$1/i = 1/i_k + 1/B\omega^{1/2}, \quad (8)$$

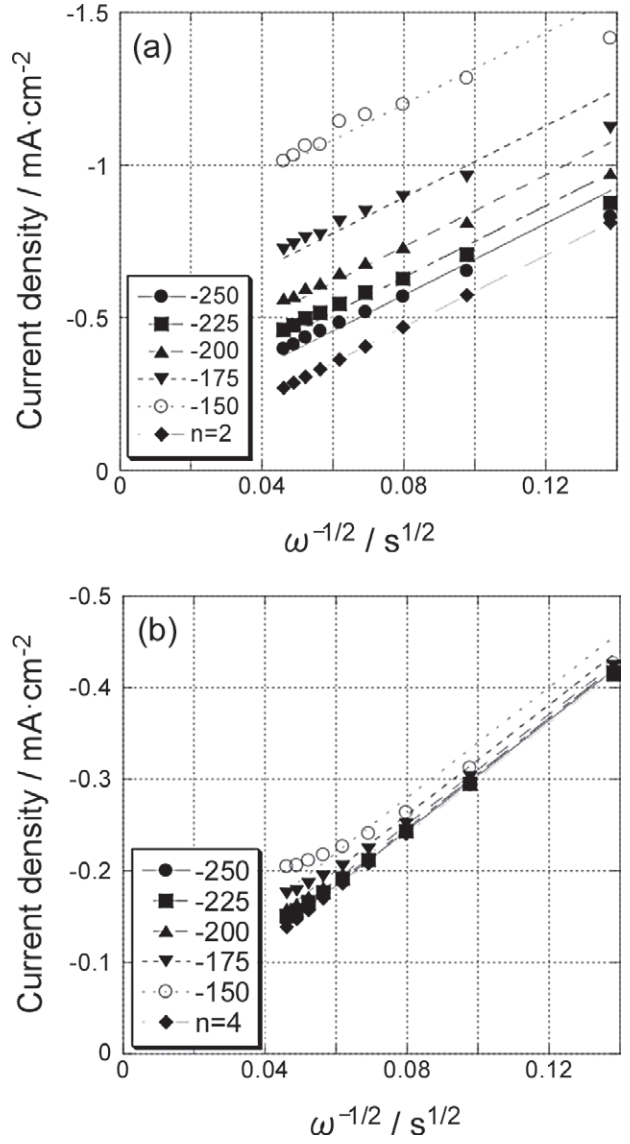

Figure 6. Koutecky–Levich plots for the polarization curves (figure 4) of the 5-layer GNC electrode (a) before and (b) after Pd deposition.

where i_k is the current in the absence of any mass transfer, which is given by

$$i_k = nFAkCo_2{}^*. \tag{9}$$

Therefore, a plot of $1/i$ versus $1/\omega^{1/2}$ should be linear and can be extrapolated to $1/\omega^{1/2} = 0$ to yield $1/i_k$. Then, the rate constant, k, can be obtained from equation (9). Figure 6 shows the K–L plots for the 5-layer GNC electrode (a) before and (b) after Pd deposition based on the data shown in figure 4. The slopes of the K–L plots of the former and the latter agree with those expected for the 2-electron and 4-electron reduction processes, respectively. The kinetic current, i_k, which is related to the reaction rate constant k, can be obtained from the intercept of the K–L plots for various potentials.

Figure 7 shows the mass transfer corrected Tafel plots, i.e. log i_k versus potential, of the 5-layer GNC electrodes before (open symbols) and after (solid symbols) Pd deposition

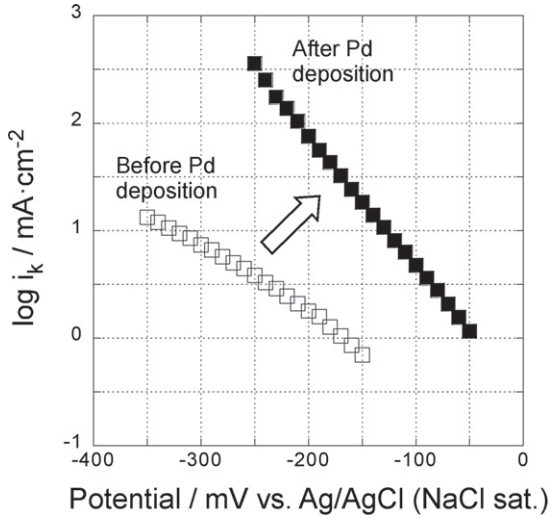

Figure 7. Potential dependence of reaction rate constants of the 5-layer GNC electrode, measured in a 0.1 M KOH solution before (open symbols) and after Pd deposition (solid symbols).

in a 0.1 M KOH solution. The Tafel slopes decreased from 150–170 mV decade^{-1} before Pd deposition to about 80 mV after deposition, reflecting the change in the ORR mechanism from 2-electron to 4-electron process, even though the Pd coverage was only about half a monolayer.

3.4. Catalytic activity of the multilayer of bare and Pd modified GNC electrodes in acidic solution

Figure 8 shows the polarization curves of the 5-layer GNC electrode deposited on a RDE. The curves were measured after 35 oxidative desorption cycles, before (figure 8(a)) and after (figure 8(b)) Pd deposition, in an oxygen saturated 0.1 M H_2SO_4 solution, at a scan rate of 10 mV s^{-1} and rotation rate between 500 and 4500 rpm as indicated in the figures. Before Pd deposition, cathodic current started to be observed at around 250 mV and increased as the electrode potential became more negative. Limiting currents were, however, not observed in this solution as current due to hydrogen evolution started to flow. This result agrees with the previous reports that the Au electrode has low electrocatalytic activity for the ORR in acidic solutions [42–46].

After Pd deposition, cathodic current started to be observed at around 550 mV and saturation was observed when the electrode potential became more negative than about −50 mV. The enhancement effect of Pd was more significant in a 0.1 M H_2SO_4 solution as the onset potential for the ORR shifted positively by about 300 mV in a 0.1 M H_2SO_4 solution, whereas the shift was only about 100 mV in a 0.1 M KOH solution.

Figure 9 shows the Levich plot for the GNC multilayer electrode after Pd deposition using the data at −100 mV of figure 4(b). A linear relation corresponding to the 4-electron ORR process was obtained. The Levich plot cannot be shown for the electrode before Pd deposition because no limiting currents were observed.

Figure 10 shows the K–L plots for the 5-layer GNC electrode (a) before and (b) after Pd deposition using the data

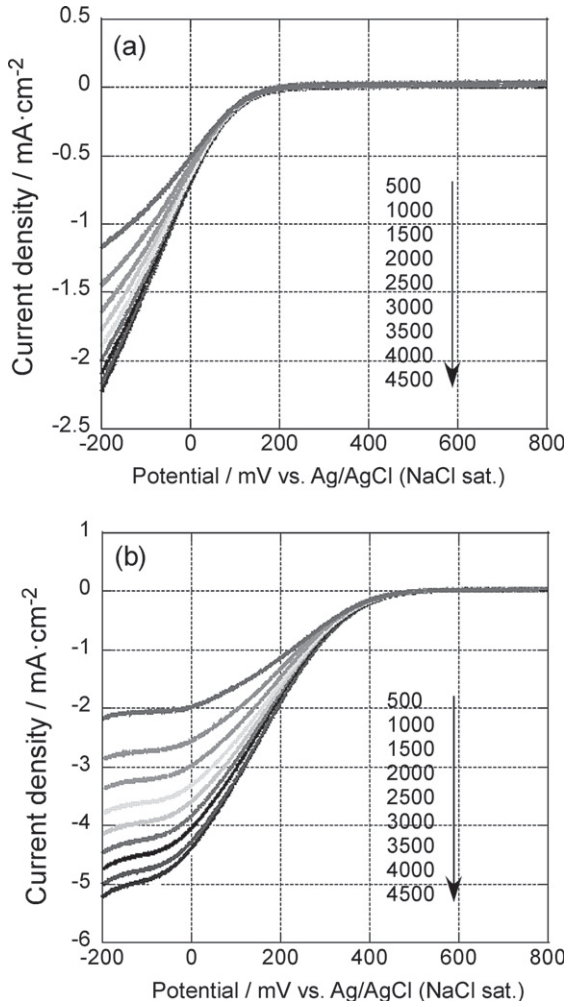

Figure 8. Rotation rate dependent polarization curves of the 5-layer GNC electrode measured after 35 oxidative desorption cycles in an oxygen saturated 0.1 M H_2SO_4 solution at a scan rate of 10 mV s^{-1}, (a) before and (b) after Pd deposition.

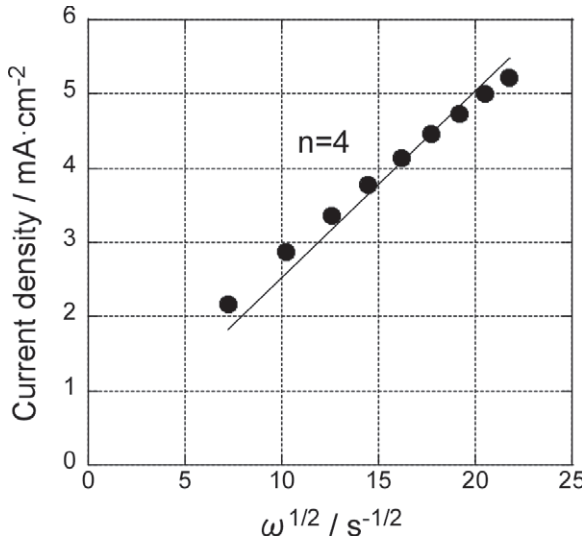

Figure 9. Levich plot for the GNC multilayer electrode at −100 mV after Pd deposition (figure 8(b)). Solid line is a fit by a 4-electron process.

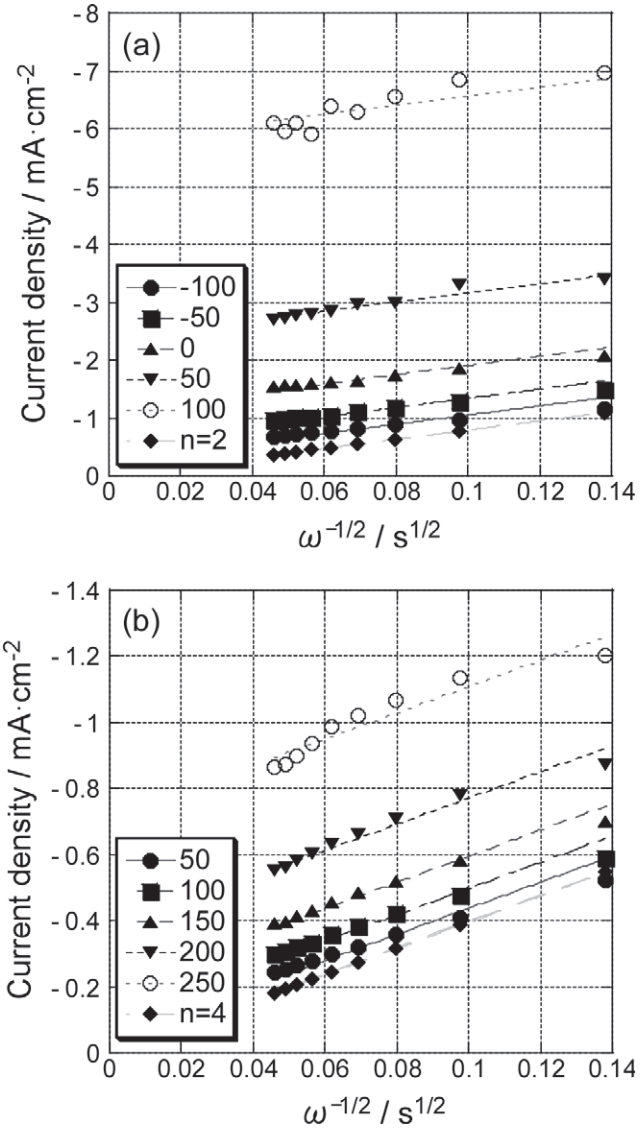

Figure 10. Koutecky–Levich plots for the polarization curves (figure 8) of the 5-layer GNC electrode (a) before and (b) after Pd deposition.

at various potentials of figure 8. The slopes of the K–L plots of the former and the latter agreed with those expected for the 2-electron and 4-electron reduction processes, respectively. Thus, although the Levich plot could not be obtained for the GNC electrode before Pd deposition, the K–L plots confirmed that the ORR in a 0.1 M H_2SO_4 solution proceeded via 2-electron and 4-electron processes at the GNC electrode before and after Pd deposition, respectively.

$$O_2 + 2H^+ + 2e^- \rightarrow H_2O_2, \tag{10}$$

$$O_2 + 4H^+ + 4e^- \rightarrow 2H_2O. \tag{11}$$

Figure 11 shows the mass transfer corrected Tafel plots (log i_k versus potential) for the 5-layer GNC electrodes before (open symbols) and after (solid symbols) Pd deposition in a 0.1 M H_2SO_4 solution. Although the electrocatalytic activity was enhanced significantly by Pd deposition, the Tafel slope in

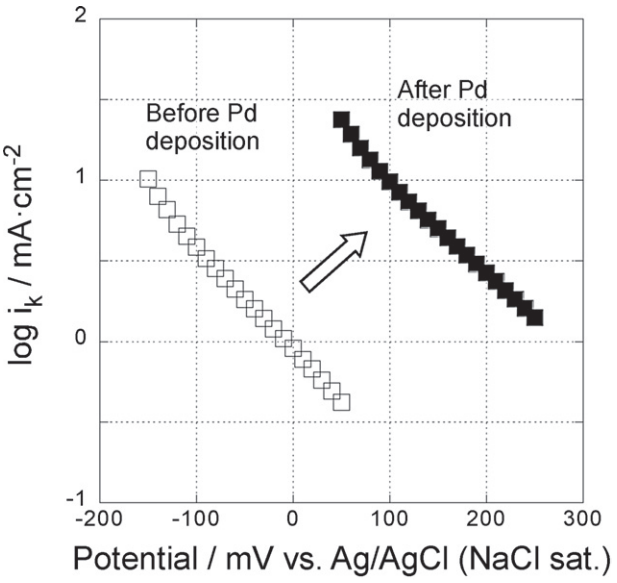

Figure 11. Potential dependence of reaction rate constants of the 5-layer GNC electrode measured in a 0.1 M H_2SO_4 solution before (open symbols) and after (solid symbols) Pd deposition.

a 0.1 M H_2SO_4 solution was not affected much. This behavior is different from that in a 0.1 M KOH solution. The slope at the Pd modified GNC multilayer electrode was larger than that at Pd metal electrode in the same solution. This may be related to the ionization of PAH. Since PAH is a polyelectrolyte of weak base with pKa of 9–11 [47], the PAH chains are fully ionized by a positive charge in a 0.1 M H_2SO_4 solution, and H^+, which is one of the reactants for the ORR in acidic solutions, is essentially rejected by PAH. Thus, the distribution of H^+ near the Pd modified GNC in the multilayer should be quite different from that near the Pd metal electrode in a H_2SO_4 solution, resulting in a relatively large Tafel slope.

4. Conclusions

Electrocatalytic activities for ORR at bare and Pd modified GNC multilayer electrodes in alkaline and acidic solutions were investigated using RDE. After the multilayer of GNCs modified with MUA SAM and PAH was constructed, the SAMs were oxidatively removed from the GNC surface by cycling potential between 0 and 1300 mV and the multilayer of bare GNC with a diameter of about 5 nm and PAH was obtained. Relatively high catalytic activity for the ORR was observed at the bare GNC/PAH multilayer electrode in an alkaline solution. Electrochemical deposition of Pd submonolayer deposition on bare GNCs in the multilayer resulted in Pd modified GNC/PAH multilayer electrode. The Pd modification enhanced the electrocatalytic activity for the ORR in both acidic and alkaline solutions. Oxygen was reduced via 2-electron and 4-electron processes at the bare and Pd modified GNC multilayer electrodes, respectively.

Acknowledgments

This work was partially supported by a Grant-in-aid for Scientific Research (A) (No. 18205016), the Global COE program (Project No. B01: Catalysis as the Basis for Innovation in Material Science) and the World Premier International Research Center (WPI) Initiative on Materials Nanoarchitectonics from the Ministry of Education, Culture, Sports, Science and Technology (MEXT, Japan).

References

[1] Adzic R R 1998 *Frontiers in Electrochemistry* vol 5 *Electrocatalysis* ed J Lipkowski and P N Ross (New York: VCH) p 197
[2] Kinoshita K 1992 *Electochemical Oxygen Technology* (New York: Wiley)
[3] Adzic R R, Strbac S and Anastasijevic N 1989 *Mater. Phys. Chem.* **22** 349
[4] Inoue H, Brankovic S R, Wang J X and Adzic R R 2002 *Electrochim. Acta* **47** 3777
[5] Kita H, Lei H-W and Gao Y 1994 *J. Electroanal. Chem.* **379** 407
[6] Kadiri F El, Faure R and Durand R 1991 *J. Electroanal. Chem.* **301** 177
[7] Watanabe M and Motoo S 1975 *J. Electroanal. Chem.* **60** 259
[8] Watanabe M and Motoo S 1975 *J. Electroanal. Chem.* **60** 267
[9] Zhang J, Vukmirovic M B, Xu Y, Mavrikakis M and Adzic R R 2005 *Angew. Chem. Int. Edn Engl.* **44** 2132.
[10] Koh S and Strasser P 2007 *J. Am. Chem. Soc.* **129** 12624
[11] Stamenkovic V R, Mun B S, Arenz M, Mayrhofer K J J, Lucas C A, Wang G, Ross P N and Markovic N M 2007 *Nat. Mater.* **6** 241
[12] Naohara H, Ye S and Uosaki K 2000 *Electrochim. Acta* **45** 3305
[13] Arenz M, Schmidt T J, Wandelt K, Ross P N and Markovic N M 2003 *J. Phys. Chem.* B **107** 9813
[14] Climent V, Markovic N M and Ross P N 2000 *J. Phys. Chem. B* **104** 3116
[15] Uehara H, Okawa Y, Sasaki Y and Uosaki K 2009 *Chem. Lett.* **38** 148
[16] Naohara H, Ye S and Uosaki K 2001 *J. Electroanal. Chem.* **500** 435
[17] Takahasi M, Hayashi Y, Mizuki J, Tamura K, Kondo T, Naohara H and Uosaki K 2000 *Surf. Sci.* **461** 213
[18] Takahashi M, Tamura K, Mizuki J, Kondo T and Uosaki K 2010 *J. Phys.: Condens. Matter* **22** 474002
[19] Awatani T, Yagi I, Noguchi H and Uosaki K 2002 *J. Electroanal. Chem.* **524–525** 184
[20] Yagi I, Ishida T and Uosaki K 2004 *Electrochem. Commun.* **6** 773
[21] Uosaki K, Kondo T, Okamura M and Song W 2002 *Faraday Discuss.* **121** 373
[22] Song W, Okamura M, Kondo T and Uosaki K 2003 *Phys. Chem. Chem. Phys.* **5** 5279
[23] Song W, Okamura M, Kondo T and Uosaki K 2003 *J. Electroanal. Chem.* **554** 385
[24] Harada M, Zanetakis N, Noguchi H, Takakusagi S and Uosaki K 2008 *Trans. Mater. Res. Soc. J.* **33** 1093
[25] Song W, Okamura M, Kondo T and Uosaki K 2008 *J. Electroanal. Chem.* **612** 105
[26] Uosaki K, Sato Y and Kita H 1991 *Langmuir* **7** 1510
[27] Brust M, Wakler M, Bethell D, Schiffrin D J and Whyman R 1994 *J. Chem. Soc. Chem. Commun.* **801**
[28] Hostetler M J, Templeton A C and Murray R W 1999 *Langmuir* **15** 3782

[29] Quayum M E, Ye S and Uosaki K 2002 *J. Electroanal. Chem.* **520** 126
[30] Kondo T, Sumi T and Uosaki K 2002 *J. Electroanal. Chem.* **538–539** 59
[31] Clavilier J, Faure R, Guinet G and Durand R 1980 *J. Electroanal. Chem.* **107** 205
[32] Uosaki K, Sato Y and Kita H 1991 *Electrochim. Acta* **36** 1799
[33] Shimazu K, Yagi I, Sato Y and Uosaki K 1992 *Langmuir* **8** 1385
[34] Ye S, Haba T, Sato Y, Shimazu K and Uosaki K 1999 *Phys. Chem. Chem. Phys.* **1** 3653
[35] Lima F H B, Zhang J, Shao M H, Sasaki K, Vukmirovic M B, Ticianelli E A and Adzic R R 2007 *J. Phys. Chem.* C **111** 404
[36] Kullapere M, Jurmann G, Tennno T T, Paprotny J J, Mirkhalaf F and Tammeveski K 2007 *J. Electroanal. Chem.* **599** 183
[37] Gubbins K E and Walker R D J 1965 *J. Electrochem. Soc.* **112** 469
[38] Davis R E, Horvath G L and Tobias C W 1967 *Electrochim. Acta* **12** 287
[39] Fischer P and Heitbaum J 1980 *J. Electroanal. Chem.* **112** 231
[40] Safavi A, Maleki N, Tajabadi F and Farjami E 2007 *Electrochem. Commun.* **9** 1963
[41] Jiang L, Hsu A, Chu D and Chen R 2009 *J. Electrochem. Soc.* **156** B643
[42] Damjanovic A, Genshaw M A and Bockris J O'M 1967 *J. Electroanal. Chem.* **15** 173
[43] Wroblowa H S, Pan Y C and Razumney G 1976 *J. Electroanal. Chem.* **69** 195
[44] Zurilla R W, Sen R K and Yeager E 1978 *J. Electrochem. Soc.* **125** 1103
[45] Vilambi N R K and Taylor E J 1989 *J. Electroanal. Chem.* **270** 61
[46] Paliteiro C 1994 *Electrochim. Acta* **39** 1633
[47] Mermunt O and Barrett C J 2003 *J. Phys. Chem.* B **107** 2525